Proceedings of the Thirty-sixth (2026) International Ocean and Polar Engineering Conference www.isope.org
Orlando, Florida, USA, May 31-June 5, 2026

ISBN 978-1-880653-72-2; ISSN 1098-6189

Numerical simulation of steady turning motion of full appendage SUBOFF in horizontal plane

*Hehe Wang, Jianhua Wang, Decheng Wan**
Computational Marine Hydrodynamics Lab (CMHL), School of Ocean and Civil Engineering,
Shanghai Jiao Tong University, Shanghai, China
*Corresponding Author

ABSTRACT

In the study of submarine maneuvering performance, the numerical simulation of maneuvering motion needs to consider the ship-propeller-rudder coupling, so the difficulty is relatively high. In this paper, the full appendage SUBOFF submarine standard model and the E1619 propeller are taken as the research objects. The method of overset grids is used in the STARCCM software to simulate the steady turning motion of the submarine in the horizontal plane. The motion of hull, propeller and rudder is realized by using the built-in DFBI module of the software. Through the numerical simulation of typical working conditions of submarine self-propulsion and steady rotation in horizontal plane, the direct numerical simulation technology path of submarine maneuvering motion based on overset grid is established. The turning characteristic parameters, force and flow field information of the submarine steady turning motion in the horizontal plane are analyzed, which provides a reference for the prediction of submarine maneuverability.

KEY WORDS: SUBOFF; steady turning; overset grid; numerical simulation.

INTRODUCTION

In submarine design and performance evaluation, the steady turning characteristics in the horizontal plane are one of the core metrics for assessing its underwater maneuverability. This motion pattern directly reflects the steady-state performance of a submarine executing a turn with a constant rudder angle in the horizontal plane, including key parameters such as tactical diameter (TD), yaw rate and speed loss. It exerts a decisive influence on tactical maneuvering, obstacle avoidance capability, and navigation safety.

Historically, research on submarine maneuvering motions has relied predominantly on model testing. Overpelt et al. (2015) conducted the earliest comprehensive model tests based on the Joubert BB2 submarine model, including experiments for six degrees-of-freedom self-propulsion, drifting, and turning maneuvers, yielding a substantial set of experimental data. Carrica et al. (2016) also performed self-propulsion tests for the Joubert BB2 submarine in both deep water and near-surface conditions at the MARIN basin, along with turning and zigzag maneuvering tests, as well as vertical maneuvers such as pitching and surfacing. Furthermore, they established a corresponding methodology for the numerical simulation of submarine maneuvering.

In recent years, with advancements in computer technology and Computational Fluid Dynamics (CFD) methods, researchers have increasingly adopted CFD for related studies. Kim (2018) employed the overset grid method and a virtual propeller disk model to simulate steady turning maneuvers at 20° and 30° rudder angles under deep-water conditions. An automatic motion control system for submarine six degrees of freedom was implemented, and the CFD simulation results were compared with model test data, validating the accuracy of the numerical approach. Similarly, Han et al. (2021) utilized the overset grid method to simulate steady 20° turns to both port and starboard. They compared turning trajectories, maneuvering parameters, and forces with experimental results, verifying their numerical method. Additionally, they extended the work to simulate spatial spiral ascent maneuvers. Huang (2018) applied a body-force propeller model comb ined with overset grid technology to simulate the horizontal turning motion of the SUBOFF model equipped with both cruciform and X-form stern appendages. They provided the motion parameters during the turning maneuver and analyzed the variations in forces and moments along the hull during the steady turning phase. Guo et al. (2024) employed the overset grid method to conduct numerical simulations of the steady turning motion for the BB2 submarine in both deep and shallow water. A comparison was made between parameters such as turning radius and tactical diameter under these conditions, and the influence of the free surface on flow field characteristics, wave-making, and vortex structures during the maneuvers was investigated. Delen et al. (2023) modeled the propeller using the Moving Reference Frame (MRF) approach and performed a relatively comprehensive numerical simulation of the SUBOFF submarine horizontal turning motion via CFD. Their findings indicated that the SUBOFF model lacks directional stability at a 0° rudder angle. They also presented the relationship between submarine turning parameters and the rudder angle. Chen et al. (2024) applied the overset grid method to carry out numerical simulations for typical submarine operational conditions, including underwater straight-line sailing, turning, and horizontal zigzag maneuvers. An analysis was conducted on the flow phenomena around the submarine and the time-history variations of kinematic and dynamic parameters during these maneuvering states

In this paper, the numerical simulation of submarine maneuvering motion is carried out by using CFD. Taking the full appendage SUBOFF submarine standard model and E1619 propeller as the research object, the maneuvering motion simulation of submarine and the coupling control of hull-propeller-rudder are realized based on the multi-level dynamic overset grid method. The numerical simulation of submarine self-propelled motion and horizontal steady turning motion is carried out. On this basis, the tunning characteristic parameters, force characteristics and flow field information of the submarine steady turning motion under different rudder angles in the horizontal plane are further analyzed, which provides technical support for the prediction and evaluation of submarine maneuverability and seaworthiness and the improvement of submarine self-propelled model test technology.

METHODOLOGY

Governing equation

Numerical simulations in this paper are conducted within the STAR-CCM+ software. The flow field is calculated by solving the Reynolds-Averaged Navier-Stokes (RANS) equations. The continuity and momentum equations are:

$$\frac{\partial \bar{u}_i}{\partial x_i} = 0 \tag{1}$$

$$\frac{\partial \bar{u}_i}{\partial t} + \bar{u}_j \frac{\partial \bar{u}_i}{\partial x_j} = \bar{f}_i - \frac{1}{\rho}\frac{\partial \bar{p}}{\partial x_i} + v\frac{\partial^2 \bar{u}_i}{\partial x_j \partial x_j} - \frac{\partial \overline{u_i' u_j'}}{\partial x_j} \tag{2}$$

where: $\bar{u_i}$ is the fluid velocity vector; t is time; subscripts "i" and "j" denote coordinate components; u_i is the velocity component in the i-direction; x_i is the position in the i-direction; f_i is the force per unit mass in the i-direction; ρ is the fluid density; p is pressure; the superscript "-" denotes a time-averaged quantity; v is the kinematic viscosity of the fluid.

Turbulent flow model

The SST k-ω turbulence model, developed by Menter (1994), is employed to close the equations. This model is effective for applications involving unsteady incompressible flows. Its transport equations are:

$$\frac{\partial}{\partial t}(\rho k) + \frac{\partial}{\partial x_i}(\rho k \bar{u}_i) = \frac{\partial}{\partial x_j}\left(\Gamma_k \frac{\partial k}{\partial x_j}\right) + G_k - Y_k + S_k \tag{3}$$

$$\frac{\partial}{\partial t}(\rho \omega) + \frac{\partial}{\partial x_i}(\rho \omega \bar{u}_i) = \frac{\partial}{\partial x_j}\left(\Gamma_\omega \frac{\partial \omega}{\partial x_j}\right) + G_\omega - Y_\omega + S_\omega \tag{4}$$

where: k is the turbulent kinetic energy; ω is the specific dissipation rate; Γ_k and Γ_ω are the effective diffusivities; G_k and G_ω represent the generation of turbulent kinetic energy; Y_k and Y_ω represent the dissipation of k and ω; S_k and S_ω are source terms.

NUMERICAL SETUP

Geometry model

This study employs the fully-appended SUBOFF model, specifically designed by the Defense Advanced Research Projects Agency (DARPA) to establish a database for submarine CFD analysis software. The model consists of a bare axisymmetric hull, a sail, and four cruciform symmetric stern appendages (control surfaces). The total length is 104.5 m, and a 1:24 scale model is used for numerical simulation. The SUBOFF model is shown in Fig. 1, and its principal dimensions are listed in Table 1.

Fig. 1 Full appendage model of SUBOFF

Table 1 Principal dimension of SUBOFF model

Term	Value	Term	Value
Predecessor L_f/m	1.016	Total length, L/m	4.356
Raft body L_m/m	2.229	Longitudinal center of gravity x_G/m	2.010
Diameter of raft body D/m	0.508	Transverse center of gravity y_G/m	0
After body L_a/m	1.111	Vertical center of gravity z_G/m	0.002

The fully-appended SUBOFF model does not have a designated propeller. In this paper, the INSEAN E1619 seven-blade highly skewed propeller designed by the Italian National Institute for Naval Architecture Studies and Testing (INSEAN) is used. The geometric model is shown in Fig. 2, and the main feature columns are shown in Table 2.

Fig. 2 E1619 propeller model

Table 2 Main characteristic parameters of E1619 propeller

Number of blades	7
Diameter (mm)	485
Hub diameter ratio	0.226
Pitch at r =0.7 R (mm)	1.15
Chord at 0.75 R (mm)	6.8

Simulation of steady turning in the horizontal plane

The Dynamic Fluid Body Interaction (DFBI) module of STARCCM + can realize the six-degree-of-freedom motion of submarine numerical simulation in the computational domain. By solving the equations of motion under hydrodynamic and externally applied forces, the kinematic information of the submarine at different time instances can be obtained, facilitating the analysis of its hydrodynamic performance. The submarine steady turning simulation methods employed by Kim (2018) and Han et al (2021). are referenced. First, a target speed is set, and the corresponding self-propulsion point propeller rotation rate is determined using a PI-controller method. Then, with the rotation rate fixed, the three degrees of freedom in the horizontal plane are released. Finally, the rudder is deflected to initiate the steady turning phase. According to the different rudder angles, the horizontal plane steady turning calculation cases are divided into six, and the rudder angles (δ) are :5°, 10°, 15°, 20°, 25°, 30°, 35°. It is worth mentioning that when the rudder is turned, the steering angle of all cases is completed within one second (that is, the steering speed is different in different cases).

Computational domain and mesh

Since only the starboard turns is performed in this paper, the size of the entire cuboid background domain is: $-2 < x / L < 12$, $-1.25 < y / L < 6$, $-1.25 < z / L < 1.25$. The top boundary of the background domain is set as a pressure outlet, while the other five boundaries are set as symmetry planes. The overset grid technique is employed to simulate the hull motion in the horizontal plane. Overset interfaces are defined between the propeller/rudders and the hull, and between the hull and the background domain. Due to the use of a multi-level overset grid approach, the computational domain is structured following a three-level hierarchy: background domain, hull domain, and propeller/rudder domains, as shown in Fig. 3.

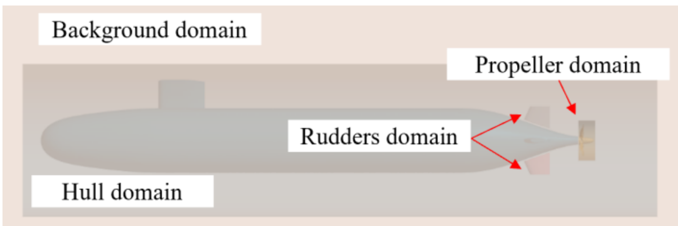

Fig. 3 Schematic diagram of computational domain

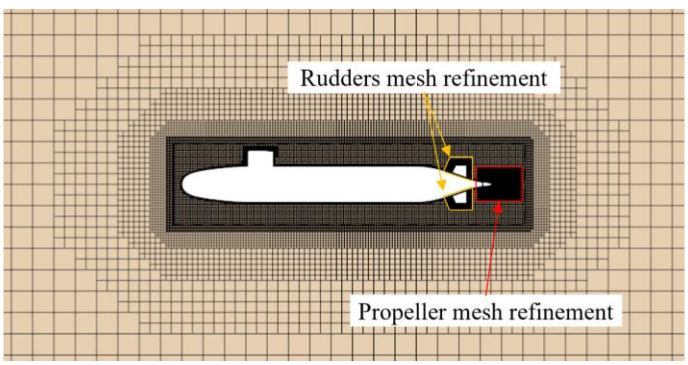

Fig.4 Grid division

It is noteworthy that flow field information is transferred between overset regions via interpolation. To minimize interpolation errors, the grid cell sizes at the overset interfaces are kept consistent. To ensure computational accuracy while reducing cell count, adaptive mesh refinement is applied near the overset interface between the background and hull domains. A trimmed mesh is used for the hull domain volume, with prism layers generated for the boundary layer. Furthermore, more refined meshing is applied at the overset interfaces between the rotating propeller/rudders and the hull for accurate simulation. Polyhedral cells are used for refinement within the rudder domains. The mesh for the computational domains is shown in Fig. 4. The total number of cells after generation is approximately 4.84 million.

VALIDATION OF NUMERICAL METHOD

In order to verify the reliability of the CFD method, the full appendage SUBOFF model direct towing tank test was first simulated. Following ITTC recommendations, the computational domain for this validation case is sized: $-2 < x / L < 1.75$, $-1.25 < y / L < 1.25$, $-1.25 < z / L < 1.25$ (L is the length of SUBOFF model). Mesh refinement is applied in the hull region to ensure accuracy. The total number of grids is 1.66 million as shown in Fig. 5.

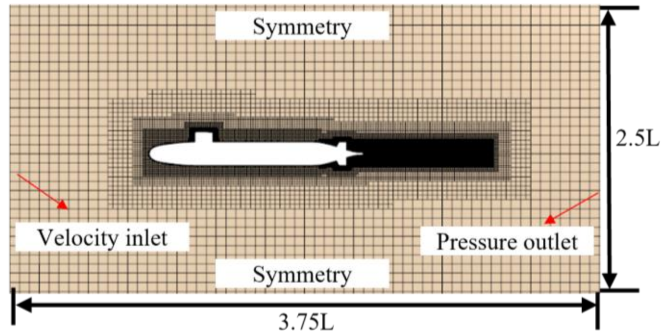

Fig. 5 SUBOFF direct test computational domain and mesh

The resistance values obtained from CFD are compared with the results from EFD (Roddy, 1990), as shown in Table 3. The comparison reveals that the relative error between the calculated and experimental resistance values is less than 10%, meeting the requirements for practical engineering applications. At the same time, the distribution of pressure coefficient along the hull calculated by CFD is compared with EFD (Huang et al, 1994). The results are shown in Fig. 6.

Table 3 Comparison between CFD and EFD results

Speed/kn	Resistance/N		Error/%
	CFD	EFD	
5.93	106.5	102.3	4.221
10.00	299.9	283.8	5.695
11.85	414.5	389.2	6.488
13.92	564.1	523.1	0.276
16.00	735.6	677.4	8.884

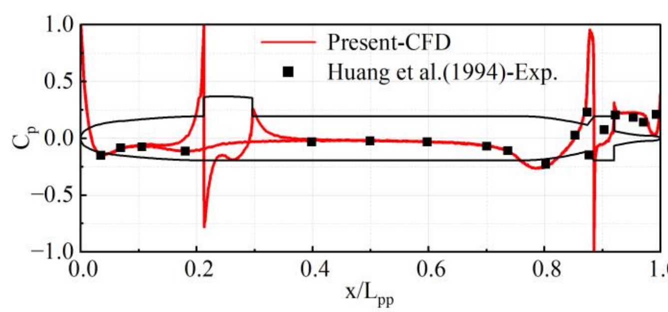

Fig.6 Comparison of pressure coefficient distribution along hull between CFD and EFD

Secondly, the open water test calculation of the propeller is carried out. The cylindrical calculation domain is adopted. The velocity inlet is $2D$ in front of the propeller disk (D is the diameter of the propeller), and the pressure outlet is $9D$ behind the propeller disk. The radius of the calculation domain is $4D$, and the boundary condition of the side of the calculation domain is set to the symmetrical surface. The calculation is carried out by overset grid method, and the calculation area is divided into inner rotation domain and outer background domain. The calculation domain is shown in Fig. 7.

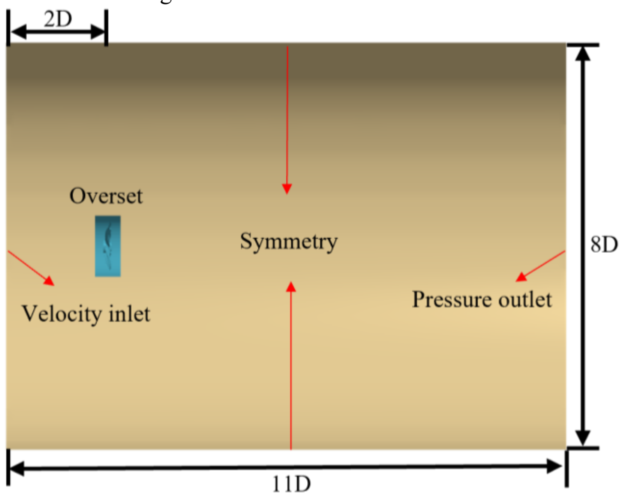

Fig. 7 E1619 open water calculation domain

The propeller speed (n) is fixed at 5rps, and the open water performance curve is calculated by changing the inflow velocity. The selection of the time step follows the time step of the propeller rotation recommended by ITTC, which is not less than 180, and the final value is 0.001s. When calculating the open water performance curve of the propeller, the field function is used to define the advance speed V_A, which is defined as the function of the advance coefficient J, and the J is defined as the iterative function($J=V_A/nD$), and the J is increased by 0.15 without 5000 iterations. The results of CFD calculation are compared with EFD (Di Felice et al. 2009), as shown in Fig. 8. Among them, K_T ($K_T=T/\rho n^2D^5$) and K_Q ($K_Q=Q/\rho n^2D^4$) are the propeller thrust coefficient and torque coefficient respectively.

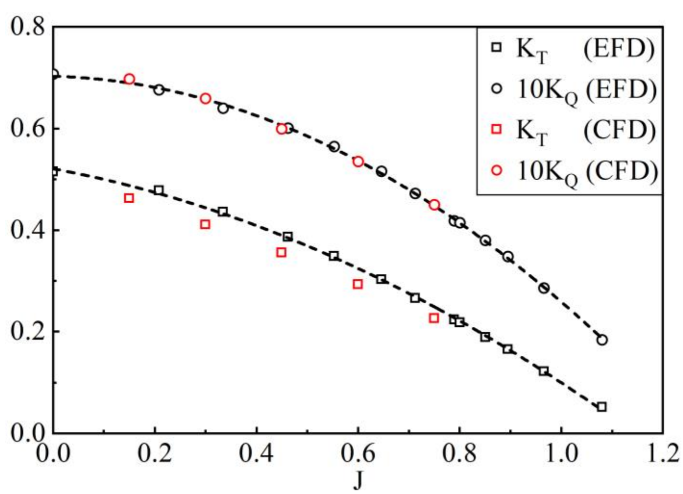

Fig. 8 Calculation results of E1619 open water characteristic curve

RESULTS AND DISSCUSSIONS

Analysis of Motion Characteristic Parameters

In the horizontal plane steady turning motion, the submarine trajectory first maintains a straight line, then bends, and finally becomes a circle. At the same time, there are some characteristic parameters to describe the turning motion, such as tactical diameter (TD), advance (Ad), transfer (Tr) and steady turning diameter (STD). The smaller the transfer and tactical diameter, the better the turning performance of the submarine, and the smaller the longitudinal distance, the more agile the steering response of the submarine to the initial moment. The dimensionless steady turning trajectory under different cases is shown in Fig. 9.

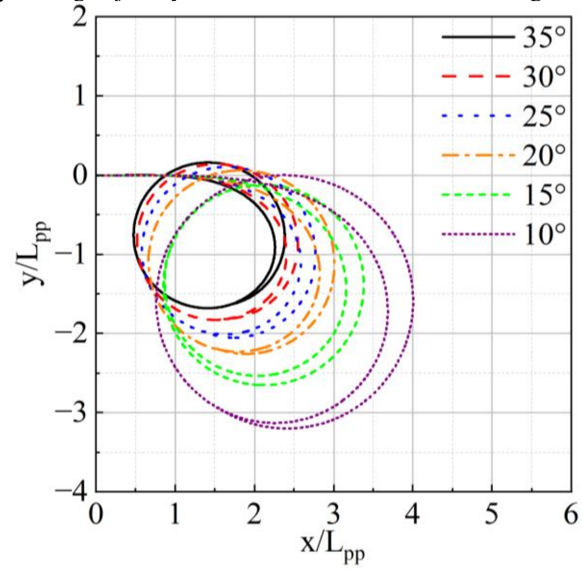

Fig. 9 Turning trajectory of submarine under different cases

Table 4 Turning characteristic parameters comparison

	Present				Delen et al. (2023)			
δ/°	Ad	Tr	TD	STD	Ad	Tr	TD	STD
10	3.633	-1.338	3.084	3.201	3.413	-1.178	2.8	2.964
15	3.156	-1.064	2.479	2.529	2.992	-1.003	2.475	2.59
20	2.755	-0.881	2.171	2.317	2.712	-0.875	2.238	2.386
25	2.507	-0.747	1.949	2.154	-	-	-	-
30	2.320	-0.646	1.763	1.968	-	-	-	-
35	2.159	-0.552	1.616	1.841	2.218	-0.648	1.838	2.129

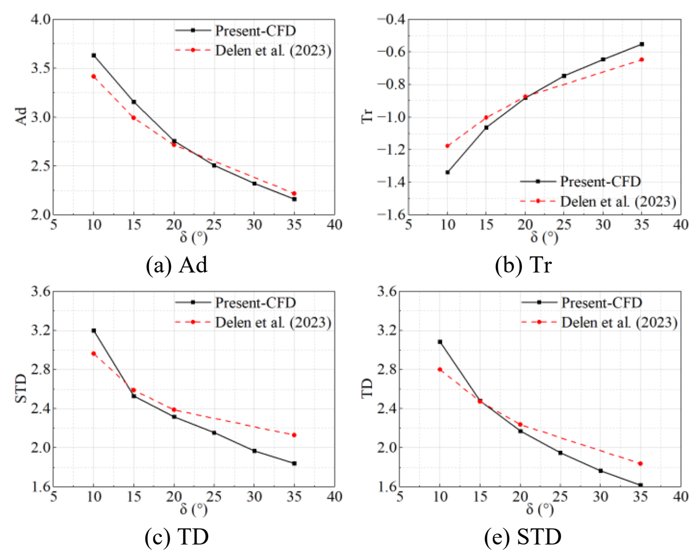

Fig. 10 Turning characteristic parameters change with rudder angle

It can be seen that under different rudder angles, the turning trajectory of the hull is first presented as a curve after turning the rudder, and then becomes a circle after the turning is stable. With the increase of the rudder angle, the circle becomes smaller after the turning is stable. Since there is no experimental data to compare the steady turning motion of SUBOFF in the horizontal plane, and there are not many numerical simulations of the motion, the turning characteristic parameters (dimensionless) calculated in this paper are given below, as shown in Table 4. And the calculation results of Delen et al. (2023) are listed for reference. It is worth noting that the hull speed in this paper is 3 m/s, compared with 2.75 m/s in the work of Delen et al. (2023). The curve of the turning characteristic parameters with the rudder angle is drawn, as shown in Fig. 10.

It can be observed that as the rudder angle increases, the absolute values of the characteristic parameters exhibit a corresponding decrease. Comparison with Delen et al. (2023) reveals that the hull speeds, though not identical, are similar, and the characteristic parameters are likewise close, indicating that the calculations in this paper are accurate. The time-history data of yaw rate and dimensionless speed loss (Defined as one minus the ratio of the hull speed to the initial speed) of submarine in turning process are shown in Fig. 11 and Fig. 12 respectively. The extreme and mean values of the yaw rate and speed loss for the submarine under different cases are presented in Table 5.

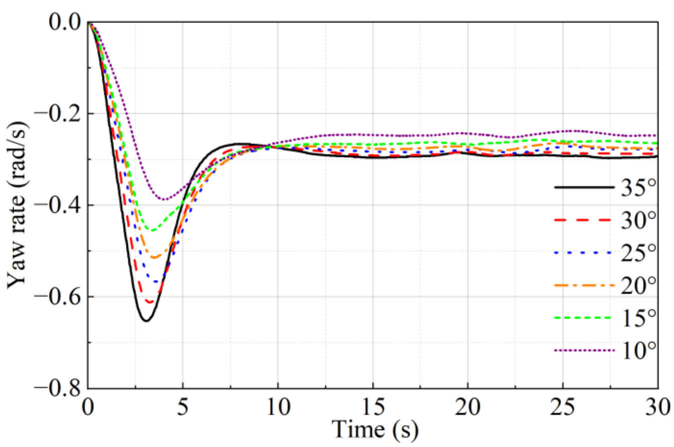

Fig. 11 Yaw rate of submarine under different cases

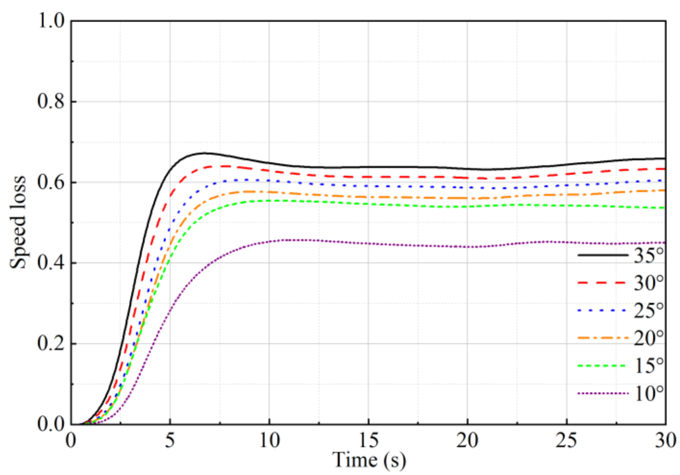

Fig. 12 Dimensionless speed loss of submarine under different cases

Table 5 The extreme and mean values of the yaw rate and the speed loss for the submarine under different cases

δ/°	Yaw rate		Speed loss	
	Extreme value	Mean value	Extreme value	Mean value
10	-0.3870	-0.2454	0.4571	0.4467
15	-0.4550	-0.2625	0.5549	0.5413
20	-0.5142	-0.2736	0.5810	0.5671
25	-0.5662	-0.2796	0.6065	0.5917
30	-0.6115	-0.2875	0.6396	0.6181
35	-0.6527	-0.2922	0.6715	0.6417

The figure shows that the trend of yaw rate change is consistent across different rudder angles: a minimum (negative peak) is reached during the transition phase, the value remains essentially constant upon entering the steady turning phase, and the absolute value of the minimum is larger. As analyzed in the following section on forces, the yaw moment acting on the submarine reaches its maximum during the transition phase, explaining the occurrence of the minimum yaw rate in this phase. It is seen that as the rudder angle increases, both the absolute value of the mean yaw rate and the absolute value of its minimum gradually increase. It is noted that during the steady turning phase, the yaw rate and the relative turning radius (*R*/*L*) are inversely proportional. The increase in yaw rate with rudder angle aligns with the trend of decreasing relative turning radius with increasing rudder angle. The trend of speed loss is also consistent across rudder angles: after rudder deflection, the speed loss gradually increases and stabilizes once the steady turning phase is reached. Combined with the force analysis below, as the rudder is turned, the resistance in the surge direction increases, leading to a decrease in hull speed. As the rudder angle increases, the mean speed loss and the maximum speed loss increase.

Force Analysis

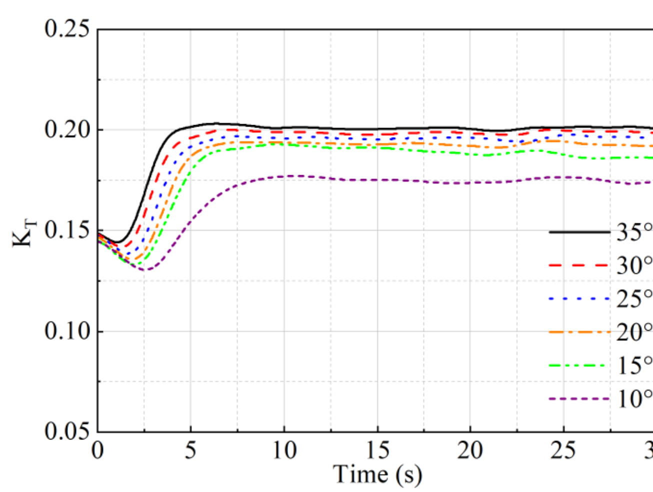

Fig. 13 Thrust coefficient (K_T) of submarine under different cases

The force of the submarine during the turning process is shown in Figs. 13~15. It can be seen that the variation trend of propeller thrust coefficient, surge force and sway force at each rudder angle reaches the extreme value in the transition phase, and then gradually changes to stability. After the rudder is turned, the flow velocity at the propeller disk surface increases temporarily. At this time, the speed change of the hull is not obvious, so the advance coefficient (*J*) increases, which leads to the decrease of the propeller thrust coefficient. Then, due to the decrease of the hull speed, the advance coefficient increases, and finally the propeller thrust coefficient increases and stabilizes. In the surge direction, the increase of the rudder angle during the rudder turning process will cause the resistance of the hull to increase, and the speed of the hull will decrease, so the resistance will also decrease, and the resistance will tend to be stable after entering the steady turning phase.

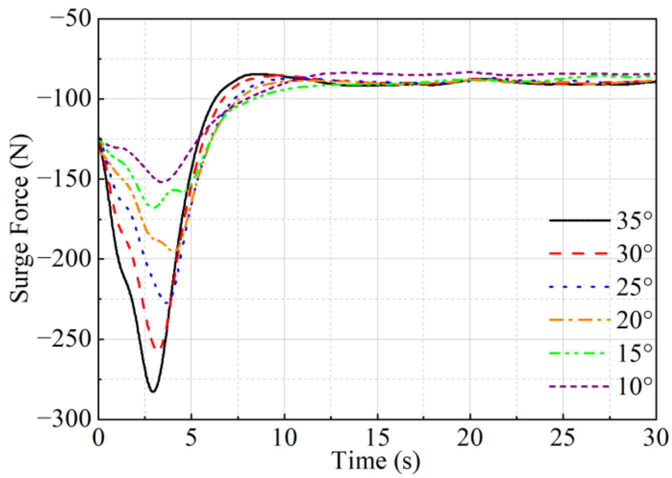

Fig. 14 Surge force of submarine under different cases

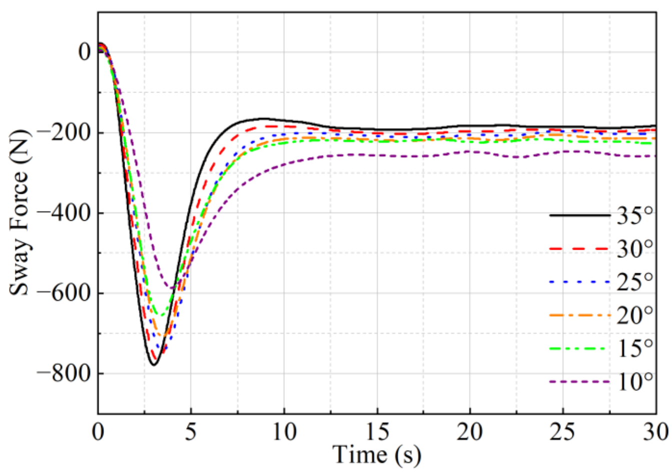

Fig. 15 Sway force of submarine under different cases

Flow Field Analysis

The velocity field around the submarine during the steady turning phase under different cases is shown in Fig.16. It can be seen from the diagram that the velocity field structure around the submarine during the steady turning phase under different rudder angles is consistent. The rudder affects the flow field behind the rudder, resulting in the inhomogeneity of the wake field on both sides of the tail. According to the Bernoulli equation, the pressure generated by the inner side of the larger wake is smaller, and the pressure generated by the outer side of the smaller wake is larger, so that the tail of the hull is subjected to a swaying force pointing to the inside. As the rudder angle increases, the speed of the submarine in the steady turning phase will gradually decrease, which is consistent with the previous analysis of the speed loss. At the same time, it can be seen that the increase of the turning rudder angle will strengthen the flow field interference behind the hull.

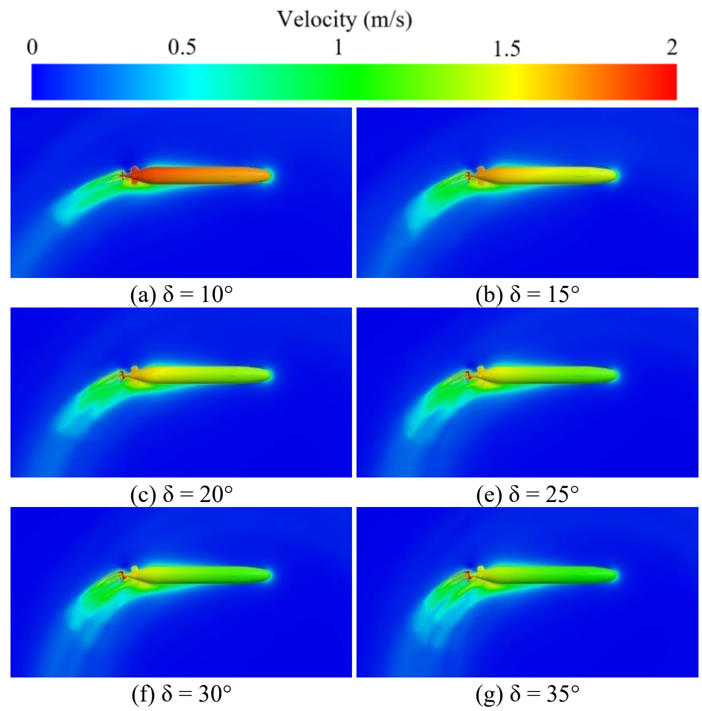

Fig. 16 The velocity field around the submarine during the steady turning phase under different conditions

CONCLUSIONS

In this study, based on STARCCM software, the steady turning motion of SUBOFF with E1619 propeller in horizontal plane is numerically simulated. The turning rudder angles are 10°, 15°, 20°, 25°, 30°, 35°, respectively. The turning characteristic parameters, force conditions and flow field around the hull are analyzed in depth. The main conclusions are as follows:

(a) In this paper, the method of overset grid is used to simulate the steady turning motion of the submarine in the horizontal plane. Firstly, the full appendage SUBOFF direct navigation resistance and E1619 propeller open water characteristic curve are verified. Secondly, the self-propulsion simulation of the submarine with propeller is carried out. After the self-propulsion point is found by the PI controller, the numerical simulation of the steady turning motion of the submarine in the horizontal plane is carried out, and the simulation method of the steady turning motion of the submarine in the horizontal plane is established.

(b) Through the numerical simulation of the steady turning motion of the submarine in the horizontal plane under different rudder angles, the turning characteristic parameters of the submarine are obtained. The accuracy of the calculation in this paper is proved by comparing with the existing literature.

(c) The hydrodynamic and dynamic characteristics of the submarine in the process of turning motion are revealed through the in-depth analysis of the force of the submarine in the steady turning motion in the horizontal plane and the flow field information around the hull.

ACKNOWLEDGEMENTS

This work was supported by the National Key Research and Development Program of China (2025YFF0519800), to which the authors are most grateful.

REFERENCES

Carrica, PM, Kerkvliet, M, Quadvlieg, FHHA, Pontarelli, M, and Martin, JE (2016). "CFD simulations and experiments of a maneuvering generic submarine and prognosis for simulation of near surface operation," *Proc 31st symposium on naval hydrodynamics*.

Chase, N, Michael, T, and Carrica, PM (2013). "Overset simulation of a submarine and propeller in towed, self-propelled and maneuvering conditions," *International Shipbuilding Progress*, *60*(1-4), 171-205.

Chen M, Zhang N, Chen JJ, Huang MM and Zeng K (2024). "Numerical simulation of submarine self-propelled model maneuvering motion based on overset grid," *Ship mechanics*, 28 (4).

Delen, C, and Kinaci, OK (2023). "Direct CFD simulations of standard maneuvering tests for DARPA Suboff," *Ocean Engineering*, *276*, 114-202.

Di Felice, F, Felli, M, Liefvendahl, M, and Svennberg, U (2009). "Numerical and experimental analysis of the wake behavior of a generic submarine propeller," *Prism*, *1*(8), 158.

Guo, EK, Wang, YJ, Cao, LS, and Wan, DC (2024). "Numerical simulation and flow field characteristics of submarine near-surface maneuvering motion ," *Hydrodynamic research and progress A*, 39 (06), 894-901.

Han, K, Cheng, X, Liu, Z, Huang, C, Chang, H, Yao, J, and Tan, K (2021). "Six-DOF CFD simulations of underwater vehicle operating underwater turning maneuvers," *Journal of Marine Science and Engineering*, *9*(12), 1451.

Huang, C, (2018). "Direct simulation of underwater vehicle maneuvering motion based on overset grids," *Wuhan University of Technology*.

Huang, T, and Liu, HL (1994). "Measurements of flows over an axisymmetric body with various appendages in a wind tunnel: the DARPA SUBOFF experimental program," *Naval Hydrodynamics, 19th Symposium USA*, Seoul, Korea, 5, 321-347.

Hunt, JC, Wray, AA, and Moin, P (1988). "Eddies, streams, and convergence zones in turbulent flows," *Studying turbulence using numerical simulation databases, 2. Proceedings of the 1988 summer program*, 89, 24555.

Kim, H (2018) "Six-DOF motion response and manoeuvring simulation of an underwater vehicle," *University of Tasmania*.

Menter, FR (1994). "Two-equation eddy-viscosity turbulence models for engineering applications,". *AIAA journal*, 32(8), 1598-1605.

Overpelt, B, Nienhuis, B, and Anderson, B (2015). "Free running manoeuvring model tests on a modern generic SSK class submarine (BB2)," *Proc Pacific International Maritime Conference,* 1-14.

Roddy, RF (1990). "Investigation of the stability and control characteristics of several configurations of the DARPA SUBOFF model (DTRC Model 5470) from captive-model experiments," *Ship Hydromechanics Department Report*, No. DTRCSHD129808.